Chemisorption geometry of $c(2\times2)$ oxygen on Cu (001) from angle-resolved core-level x-ray photoemission

S. Kono,* S. M. Goldberg,† N. F. T. Hall, and C. S. Fadley‡
Department of Chemistry, University of Hawaii, Honolulu, Hawaii 96822
(Received 8 January 1980)

The x-ray photoelectron intensity of the 1*s* core level of adsorbed oxygen in the form of a $c(2\times2)$ overlayer on Cu (001) exhibits strong angular dependence due to final-state diffraction at low electron take-off angles. The azimuthal anisotropies of the intensity, measured as $(I_{max}-I_{min})/I_{max}$, are 24%, 23%, 16%, 13%, and 18% for scans at fixed electron take-off angles of 7°, 10°, 13°, 15°, and 17° with respect to the surface, respectively. A strong sensitivity of the azimuthal pattern to the electron take-off angle is also noted. Similar azimuthal anisotropies measured on the substrate Cu 3*p* and $2p_{3/2}$ core levels are considerably stronger, with $(I_{max}-I_{min})/I_{max}\lesssim 73\%$ at electron take-off angles from 7° to 45°. Single-scattering cluster (SSC) calculations have been performed for both substrate and adsorbate core emission. The calculated azimuthal patterns for the substrate core emission show very good agreement with experiment at low electron take-off angles and reasonable agreement at high electron take-off angles, thereby verifying the applicability of the SSC model to the adsorbate core emission as well. Within several choices of the oxygen overlayer geometry tentatively proposed previously, the SSC results for the adsorbate core emission show by far the best agreement with experiment for oxygen atoms in fourfold-hollow sites, coplanar with the first Cu layer. The validity of various approximations made in the SSC model is also discussed, together with the estimated accuracy of the method.

I. INTRODUCTION

Several techniques have been developed in recent years for determining the geometries of chemisorption systems. Among these, LEED (low-energy electron diffraction) has been the most widely used for the study of ordered surface structures of substrates and adsorbates.[1] However, the determination of adsorbate geometry has not proven to be a simple task. In LEED, *I-V* curves have been measured for many combinations of adsorbate and substrate and these have been compared to kinematical and dynamical calculations for several choices of plausible geometries.[2] There are as yet not many fully decisive determinations of adsorbate geometries made with this technique, mainly because of the complexity of both the data acquisition and the multiple-scattering theory necessary at these low energies of ~50–300 eV. Several newer methods have also been brought to this field in recent years, such as valence-level angle-resolved ultraviolet photoelectron spectroscopy (ARUPS),[3] surface extended x-ray absorption fine structure (SEXAFS),[4] and ion scattering spectroscopy (ISS).[5] We present here a detailed discussion of the first application of a new technique which is based on angle-resolved x-ray photoemission (XPS) of deep core levels in adsorbates. In a recent preliminary study by Kono *et al.*[6] of the angular dependence of x-ray photoelectron intensity from the adsorbate oxygen 1*s* core level in a $c(2\times2)$ overlayer on Cu (001), it has been found that the final-state diffraction of the oxygen 1*s* photoelectron by the neighboring atoms is detectable at low electron take-off angles. In a subsequent investigation,[7] single-scattering calculations were found to describe the data very well and to permit a tentative determination of the adsorbate geometry. In this paper, a more detailed discussion of these results is presented, together with some remarks concerning the general prospects for this method.

In principle, the technique discussed here is closely related to angle-resolved core-level photoemission studies at much lower energies discussed originally by Liebsh from a theoretical point of view.[8] It was pointed out[8] that studying such localized nonbonding initial states of the adsorbate simplifies the characterization of the initial states and that the angular dependence of this photoelectron intensity, with kinetic energies comparable to LEED energies, is quite complementary to the diffraction in LEED. Woodruff *et al.*[9] and later Kevan *et al.*[10] have very recently demonstrated that this type of low-energy angular dependence does exist for several adsorbates on the Ni (001) surface and have found encouraging agreement between these results and calculations based on the multiple-scattering formalism used in LEED. However, the difference in energy between ~100 eV in these lower-energy studies and ~10^3 eV for XPS in this study leads to significant differences in the method of analysis; most notably, the simpler expedient of single scattering appears possible at higher energies.

Our experimental procedure is described in Sec. II. Section III is devoted to the description

of the single-scattering cluster formalism. In Sec. IV, the experimental results are presented, and in Sec. V, the results of the single-scattering cluster (SSC) calculations are compared with experiment. Section VI discusses the results and Sec. VII presents our overall conclusions.

II. EXPERIMENTAL PROCEDURE

The experimental apparatus has been described in detail previously.[11,12] A Hewlett Packard 5950A x-ray photoelectron spectrometer has been modified to permit computer-controlled two-axis rotations of the specimen *in situ*. A schematic drawing of the experimental geometry is shown in Fig. 1. Both the polar angle θ and the azimuthal angle ϕ associated with the electron-emission direction were varied. θ is here defined with respect to the surface and ϕ with respect to the [100] direction. Full ϕ rotations of $>360°$ were possible. Polar rotations were performed about an axis perpendicular to the plane containing the x-ray incidence and the electron-exit directions. Azimuthal rotations were about the surface normal. An accuracy of $\pm1°$ was obtained in both angles. The solid angle accepted by the analyzer has been determined by electron trajectory calculations to be a cone of 3.5° half-angle.[12] Monochromatized Al $K\alpha$ radiation at 1486.6 eV was used for excitation. The angle between the x-ray incidence and electron-emission directions was fixed at 72° (cf. Fig. 1). A separate UHV sample preparation and analysis chamber was connected to the analyzer through a straight-through valve with a bellows transfer system, thus providing full UHV conditions during all phases of the experiments. A copper single crystal was mechanically polished to within ±0.5° of (001) as judged from the back-diffraction Laue pattern. After the final mechanical polishing with 0.05-μm Al_2O_3 powder, the single crystal was chemically etched briefly with $2N$ HNO_3 to reduce structural disorder near the surface. Cycles of Ar-ion bombardment at 400 V and 350 °C and annealing for ~20 min at 450 °C in vacuum were employed to obtain a clean and ordered crystal surface. Base pressures of 5×10^{-11} to 2×10^{-10} Torr were kept in both the sample and the analyzer chambers. No detectable contaminant peaks were found in XPS spectra after the crystal cleaning.

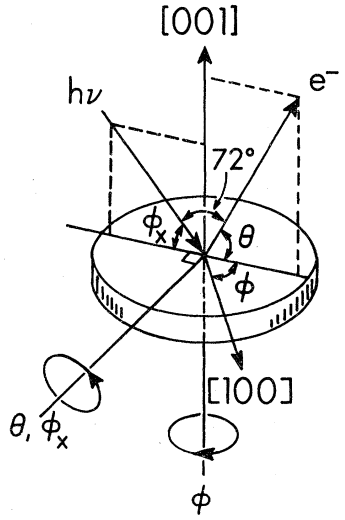

FIG. 1. Schematic illustration of the experimental geometry, with various pertinent angles defined. Rotation of the specimen on both axes noted was possible.

The oxygen chemisorption state was formed by O_2 exposures of 1200 L (1 L $=10^{-6}$ Torr sec) at 10^{-6} Torr and 25°C. LEED measurements were made in a separate chamber on the same single crystal with the same exposure conditions and these showed a $c(2\times2)$ overlayer structure, as expected from prior studies of this system.[13-16] XPS spectra of the O 1s core level due to the chemisorbed oxygen showed rather narrow and symmetric peaks with full width at half maximum (FWHM) ≈1.3–1.4 eV at $\theta=10°$ and their shapes and positions did not change during the duration of a given azimuthal scan. For a given θ and ϕ, the O 1s/Cu 3s intensity ratio changed by less than the experimental uncertainty of ~10% over the course of an azimuthal scan. This suggests a stable, well-defined chemical state of the chemisorbed oxygen.

The integrated intensities of the core-level peaks were evaluated so as to include only the elastically scattered electrons by subtracting inelastic background in a self-consistent way as applied previously to XPS valence-band spectra.[17] A wide range of background level measurement of ~3.5 eV was made on both the high- and the low-energy sides of the main peak to minimize the statistical error in the peak-intensity evaluation.

A strong diffraction peak in the substrate Cu $2p_{3/2}$ core-level intensity directly along the [001] direction was used to define the polar-angle scale in the experiment and was found to be only 0.4° different from the surface normal, in agreement with the Laue diffraction pattern. In addition, similarly strong diffraction peaks of the Cu 3p core-level intensities along the four equivalent ⟨101⟩ directions at $\theta=45°$ were used to define the azimuthal orientation. The presence of these strong diffraction peaks in the Cu core levels also verified the presence of a very high degree of surface order of the crystal.[11] In fact, the degree of azimuthal anisotropy for Cu 3p at $\theta=45°$,

which reached as high as $(I_{max}-I_{min})/I_{max}=0.73$, was found to be very sensitive to the method of cleaning and the duration and temperature of annealing.

Azimuthal scans at various polar angles were carried out in 4.5° steps with full 360° rotation plus an overlap of several degrees to check instrument stability. Typical times required for an adsorbate azimuthal scan were 15 h. Sufficient statistics were obtained with a single azimuthal scan for the Cu core levels. Additional scans were required to obtain reasonable statistics for the much weaker oxygen 1s level, although each individual scan was found to reproduce all fine structures reported here. The core peaks studied here and their relevant kinetic energies (measured relative to the bottom of the condution bands inside the crystal) and de Broglie wavelengths were as follows: Cu $2p_{3/2}$ −563 eV, 0.52 Å; Cu $3p$ −1420 eV, 0.33 Å; and O 1s −965 eV, 0.39 Å.

III. SINGLE-SCATTERING CLUSTER CALCULATIONS

A. General formalism of the single-scattering calculations

The single-scattering model we shall use here can be described as a superposition of the primary wave excited from a given site and those waves scattered once by atoms at other sites. As shown schematically in Fig. 2, the primary photoelectron wave from a given core level is assumed to be a spherical wave emanating in all directions but with an amplitude that is modulated by the photon polarization vector $\hat{\epsilon}=\vec{\epsilon}/\epsilon$ according to the core-level differential photoelectric cross section.[18,19] Some parts of the wave reach the detector without suffering any scattering along the electron wave vector $\vec{k}$. The scattered waves originate for scatterer atoms j at position $\vec{r}_j$ and reach the detector with scattering angles of θ_j, after perhaps undergoing attenuation due to inelastic scattering or slight refraction at the surface potential barrier. Thus a scattering angle of $\theta_j\sim0°$ corresponds to forward scattering. The problem to be solved is the calculation and superposition of all the waves at the detector point.

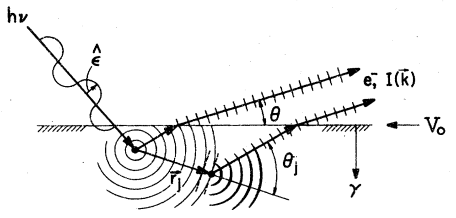

FIG. 2. Schematic illustration of the single-scattering model. $\hat{\epsilon}$ is a unit polarization vector, $\vec{r}_j$ the position of the jth scatterer, θ_j the scattering angle, θ the polar angle of observation, $I(\vec{k})$ the photoelectron intensity along an observed electron wave vector $\vec{k}$, V_0 the inner potential, and γ the inelastic attenuation coefficient equal to $1/(2\Lambda_e)$.

The model to be employed here is based on two previous studies[18,20] but also contains certain special extensions appropriate to the XPS problem at hand. Lee[18] has derived an equation for the photoemission rate $I(\vec{k})$ of adsorbate core emission in connection with surface extended x-ray absorption fine structure as follows:

$$I(\vec{k})=C\left|\hat{\epsilon}\cdot\hat{k}+\sum_j\frac{\hat{\epsilon}\cdot\hat{r}_j}{r_j}f_j(\theta_j)e^{ikr_j}(1-\cos\theta_j)\right|^2, \quad (1)$$

where C is a factor slowly varying with excitation energy which has no angular dependence for a spherically distributed initial state and $f_j(\theta_j)$ is the complex scattering factor of the jth atom as given by $f_j(\theta_j)=|f_j(\theta_j)|\exp[i\Psi_j(\theta_j)]$. No inelastic electron scattering or vibrational motion of the atoms is included in this derivation. The important approximations made here are (1) that the differential cross section for excitation can be calculated by using a plane-wave final-state $\exp(i\vec{k}\cdot\vec{r})$ and thus has an angular dependence of $\hat{\epsilon}\cdot\hat{k}$ for emission from a spherically symmetric subshell[21] and (2) that the primary photoelectron wave can be approximated by a plane wave at the time it reaches the scatterers (the "small-atom" approximation).[22] As Lee has mentioned, Eq. (1) has the simple meaning that the plane wave emitted towards $\vec{r}_j$ has an amplitude factor of $\hat{\epsilon}\cdot\hat{r}_j/r_j$ and it is then scattered in the $\vec{k}$ direction with an additional amplitude factor of $f_j(\theta_j)$. The phase $kr_j(1-\cos\theta_j)$ is simply related to the path-length difference between the primary and the scattered waves. McDonnell *et al.*,[20] in attempting to treat angle-resolved Auger emission; have taken into account the inelastic scattering of the electrons and the vibrational motion of the atoms in their single-scattering formalism. The inelastic-scattering effect is introduced as an isotropic attenuation of electron intensity due to a finite electron mean free path Λ_e. The thermal vibration effect is introduced via a Debye-Waller factor $W_j=\exp[-2k^2(1-\cos\theta_j)\overline{U}_j^2]$, where $\overline{U}_j^2$ is the one-dimensional mean-squared displacement of the jth atom with respect to the emitter. Their resulting expression for the Auger electron rate $I(\vec{k})$ in the $\vec{k}$ direction is

$$I(\vec{k})\propto\left|e^{-\gamma L}+\sum_j\frac{f_j(\theta_j)}{r_j}W_j e^{-\gamma L_j}\exp[ikr_j(1-\cos\theta_j)]\right|^2 + \sum_j\frac{|f_j(\theta_j)|^2}{r_j^2}(1-W_j^2)e^{-2\gamma L_j}, \quad (2)$$

where $\gamma=1/(2\Lambda_e)$, and L is the relevant path length

from emitter to surface and L_j is that from emitter to jth scatterer to surface.[20] The effects of inelastic scattering appear as attenuations on the primary and scattered amplitudes as $\exp(-\gamma L)$ and $\exp(-\gamma L_j)$, respectively. The Debye-Waller factor W_j appears as a damping factor on each coherent scattering term in the first $\sum_j$ term. The second $\sum_j$ term is the so-called thermal diffuse-scattering (TDS) (Ref. 23) term in which no coherent superposition of waves exist. The TDS term also can be viewed simply as correcting the first $|\cdots|^2$ for the incorrect inclusion of Debye-Waller attenuation in terms representing squares of wavelets originating on the same atom j. The thermal diffuse-scattering term thus increases as $\overline{U}_j^2$ increases, in contrast with the coherent-scattering term. In the energy range of XPS, the finite electron mean free path and the thermal vibrations of atoms may be important. Therefore we need to combine Eq. (1) and Eq. (2). Also the random polarization of the incident x-ray radiation in our experiment implies further modification. Although we will not rigorously derive this equation, the following directly results as a reasonable formula within the single-scattering model for our experiment[7]:

$$I(\vec{k}) \propto \int \left| \hat{\epsilon}\cdot\hat{k}e^{-\gamma L} + \sum_j \frac{\hat{\epsilon}\cdot\hat{r}_j}{r_j} f_j(\theta_j) W_j e^{-\gamma L_j} \exp[ikr_j(1-\cos\theta_j)] \right|^2 d\hat{\epsilon} + \sum_j \int (\hat{\epsilon}\cdot\hat{r}_j)^2 \frac{|f_j(\theta_j)|^2}{r_j^2} (1-W_j^2) e^{-2\gamma L_j} d\hat{\epsilon}\,, \tag{3}$$

where the integration with respect to $\hat{\epsilon}$ is over 360° in the plane of polarization of the incident x rays. Expanding the absolute square in Eq. (3) and integrating with respect to $\hat{\epsilon}$ yields, in place of $\hat{\epsilon}\cdot\hat{k}$ and $\hat{\epsilon}\cdot\hat{r}_j$, functions like $\cos\eta_{k,r_j}$ and $\cos\eta_{r_j,r_i}$ in cross terms, where η_{k,r_j} or η_{r_j,r_i} are the angles between $\vec{k}$ and $\vec{r}_j$ or $\vec{r}_j$ and $\vec{r}_i$ as projected onto the plane of polarization. Specifically, the final result is

$$I(\vec{k}) \propto e^{-2\gamma L}\sin^2\theta_k + \sum_{j,i} I_j I_i W_j W_i \cos\eta_{r_j,r_i}\cos(\delta_j - \delta_i)$$

$$+ 2\sum I_j e^{-\gamma L} W_j \sin\theta_k \cos\eta_{k,r_j}\cos\delta_j + \sum_j I_j^2(1-W_j^2)\,, \tag{4}$$

where $I_j = |f_j(\theta_j)|\sin\theta_{r_j}\exp(-\gamma L_j)/r_j$ and $\delta_j = kr_j(1-\cos\theta_j) + \Psi_j(\theta_j)$ and θ_k or θ_{r_j} are the angles between the polarization plane and $\vec{k}$ or $\vec{r}_j$. However, detailed numerical calculations have demonstrated that, because of the strong forward peaking of $f_j(\theta_j)$ in the XPS energy range (as will be discussed in the next section), an approximation with $\cos\eta_{k,r_j} = \cos\eta_{r_j,r_i} = 1$ gives no noticeable differences in comparison with the exact calculation. Thus Eq. (4) can be simplified as

$$I(\vec{k}) \propto \left| e^{-\gamma L}\sin\theta_k + \sum_j I_j W_j \exp\{i[kr_j(1-\cos\theta_j) + \Psi_j(\theta_j)]\} \right|^2 + \sum_j I_j^2(1-W_j^2)\,. \tag{5}$$

Equation (5) can thus be used directly for adsorbate core photoemission, but for substrate core photoemission, a summation over all possible types of emitter sites inward from the surface has to be carried out.

The only effect of the surface is assumed to be a slight direction change due to electron refraction as described by

$$\tan\theta = (\sin^2\theta' - V_0/E_k)^{1/2}/\cos\theta'\,, \tag{6}$$

where V_0 is the inner potential, E_k is the kinetic energy of the electron inside the solid, and θ' or θ are the polar angles with respect to the surface inside or outside of the solid, respectively.[24]

B. Electron-atom scattering at energies of ~10^3 eV

In order to clarify certain approximations possible in our single-scattering model, the nature of electron-atom scattering at typical XPS electron energies of ~10^3 eV should be discussed. The scattering of an incident plane wave by a spherically symmetric potential is a classical problem in quantum mechanics which is conventionally described by the partial-wave method with a complex scattering factor $f_j(\theta_j) = |f_j(\theta_j)| \times \exp[i\Psi_j(\theta_j)]$, and various calculations of such scattering factors have been made.[25-27] For most of the atoms in the first to third rows of the Periodic Table, the magnitude $|f_j(\theta_j)|$ at an electron energy of ~10^3 eV shows a peak at $\theta_j = 0°$ of 3–5 Å with a relatively narrow FWHM intensity of 10°–20°.[25-27] This peak is accompanied by only very weak backscattering with a strength of only ~0.2 Å at higher angles and with minor oscillations in θ_j. This shows that the scattered-electron intensity is mainly very strongly peaked in the forward direction. We now consider a quantitative example for clarification.

In the case of scattering of core-level x-ray

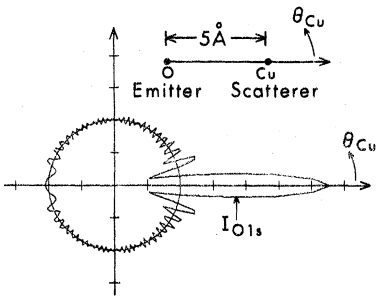

FIG. 3. Calculated angular dependence of photoelectron intensity excited by Al $K\alpha$ radiation from an O 1s level as scattered by a Cu atom at a distance of 5 Å. No effects due to inelastic scattering, thermal vibration, or radiation polarization are included in using Eq. (5) for this case, and $f_j(\theta_j)$ was taken from Ref. 26. The circle represents the spherical primary-wave electron intensity, although normalizing of total primary and total scattered intensities so as to be equal has not been done.

photoelectrons, the primary wave is a spherical wave emanating from the excited atom modulated by any polarization dependence of the photoelectric cross section.[18,19] The small-atom approximation[22] is then made by treating the spherical wave as a plane wave moving from the emitter to the scatterer and thus arriving at Eq. (5) in Sec. III A. Figure 3 shows some quantitative results obtained from Eq. (5) for the scattering of oxygen 1s photoelectrons with a kinetic energy of 965 eV by a single copper atom. The O–Cu distance was taken to be 5 Å. In this calculation, $f_j(\theta_j)$ was taken from Ref. 26, and for simplicity, inelastic scattering, thermal vibrations, and polarization effects are neglected. The calculated electron intensity shows sharp peaking along the O–Cu axis with a FWHM of 12° and a peak intensity that is ~3 times stronger than the primary intensity. Also, one observes a fine oscillatory behavior in θ_j due to interference between the primary and the scattered waves. The intensity of the forward peaking is found to be a function of the O–Cu distance in that the peak maximum reduces to only ~50% of the primary at a distance of 15 Å. On the other hand, it is almost 10 times the primary at an O–Cu distance of 2 Å. This suggests that the final-state scattering effect described by this model is in principle a small-scattering-angle and short-range effect. Thus, it is expected that, for adsorbate core emission, grazing electron take-off angles with respect to the surface will be those for which such scattering effects will be most easily detected. Adsorbates with lower atomic number like oxygen have smaller scattering power compared to typical transition-metal substrates,[25,26] so that the scattering of adsorbate core photoelectrons by other adsorbates is an even shorter-range effect. One other important aspect to be pointed out is that, for a *molecular* adsorbate system, the distance between emitter and scatterer may be short enough that the scattering of a core photoelectron from one component atom of the molecule by the other component atom may be comparable to or greater than that of the substrate. This has been demonstrated recently for CO adsorbed on Ni (001) by considering the C 1s intensity as scattered by oxygen.[28] However, we note that the small-atom approximation may not be fully valid for this case[28] and also that the deviation of the scattering potential from spherical symmetry may be important.[29] In any case, the qualitative expectation for deviations from the small-atom limit is only that they will reduce the strength of forward scattering for nearest-neighbor atoms, but not that the overall predicted anisotropy patterns should be greatly altered.

C. Input parameters and computation procedure

The complex scattering factor $f_j(\theta_j)$ is a key part of this model, and for this study, we have used values obtained by Pendry based on 21 partial-wave phase shifts for copper and oxygen scatterers at the energies of interest here.[1,27,30] In order to reproduce the environment of the chemisorption system as nearly as possible, the phase-shift calculations were made for oxygen embedded with copper in a sodium chloride lattice.[27,30] The copper phase shifts obtained in this way were almost identical to those obtained from the pure metal.[27] Also, to test the sensitivity of this type of calculation to the type of scattering factor used, we have separately utilized the purely atomic scattering factors of Fink and Ingram.[26] These atomic scattering factors are found to be somewhat different from those of Pendry in that, for $\theta_j \lesssim 10°$, the atomic $|f_j(\theta_j)|$'s are about two times as large as Pendry's values and the phases $\Psi_j(\theta_j)$ are less than those of Pendry by ~15°. For $\theta_j > 10°$, the two types of scattering factors are found to be almost identical. However, even with these differences, the calculations for both substrate and adsorbate core emissions using the atomic scattering factors yield results essentially identical to Pendry's for both the form of the anisotropies and their overall magnitudes as judged by $\Delta I/I_{max}$. The reason for this is that the experimental anisotropies are measured for $\theta \gtrsim 10°$, so that scattering angles $\theta_j \gtrsim 10°$ are involved, and for these, the two f_j's are nearly identical. Thus the exact choice of method in computing $f_j(\theta_j)$ does not seem to be critical to the predicted azimuthal patterns. We will also show from comparisons between experiment and theory in Sec. V that the *effective*

scattering factor in a solid at high energy appears to be less than the calculated value. That this may be the case can be deduced from discrepancies between experiment and theory as to certain relative peak intensities in the azimuthal patterns that can be reduced by reducing $|f_j(\theta_j)|$ empirically. Also, the overall degrees of anisotropy in the experimental patterns are always found to be less pronounced than predicted by theory. There may be several causes for this suppression of structures: (1) anisotropic inelastic scattering, such that increased scattering occurs near atomic centers, for example, due to localized d-state excitations,[7] (2) deviations from the small-atom approximation, such that wave curvature for nearest-neighbor scattering must be included,[22,28] (3) nonharmonic thermal vibration effects which are not included in the Debye-Waller factors, (4) multiple-scattering effects, and (5) imperfections in the specimen conditions, as for example, surface irregularities or multiple adsorption sites. In order to crudely approximate these effects, we have thus tried some calculations in which $f_j(\theta_j)$ was reduced to $f_j(\theta_j)/\beta$ (with $\beta \geq 1$). The case $\beta = 2$ is, in fact, empirically found to give the best agreement with experiment for all the *substrate* cases studied as to peak *positions* and relative peak *heights*. However, the nonadjusted $\beta = 1$ still shows the same degree of agreement as to peak *positions*, so that this reduction in the strength of $f_j(\theta_j)$ is not a major correction. None of our conclusions concerning structures would be changed by using only $\beta = 1$ theoretical results.

A reasonable estimate of the electron mean free path Λ_e representing isotropic inelastic scattering in copper metal is 15.0 Å at $E_k = 1482$ eV with a scaling as $(E_k)^{1/2}$.[31] Trial calculations showed however that this could be varied by $\pm\frac{1}{4}$ of the value without yielding any essential changes for copper substrate emission. For adsorbate core emission, Λ_e in the overlayer might be different from that of pure copper. However, trial calculations showed less sensitivity to changes of Λ_e in the overlayer region because the scattering power of oxygen is much weaker, that is, only neighbor oxygens very close to the emitter produce significant scattering, so changing the inelastic "cutoff" function outside these has little effect. Thus, a Λ_e of pure copper should also be adequate in the oxygen overlayer region. The surface cutoff of inelastic scattering was arbitrarily assumed to occur in a plane located at the Cu hard-sphere radius of 1.28 Å above the atomic centers in the first Cu layer. However, this choice is not significant as long as the emitter lies near or inside the surface cutoff, since the attenuation in the layer region between the surface cutoff and the emitter causes the same attenuation factor for both the primary and the scattered waves.

A reasonable inner potential V_0 for the Cu (001) surface is 14.1 eV as based on the sum of the theoretical Fermi energy relative to the bottom of the conduction bands and the experimental work function.[32] As calculated from Eq. (6), this results in a refraction of electrons at $E_k = 965$ eV of $\Delta\theta = 2.8°$ for an internal $\theta' = 10°$. The full inner potential also may not be appropriate for adsorbate emission,[1] as the emitter site may be somewhere in the region of the potential slope at the surface, and thus added calculations at the extreme limit of $V_0 = 0.0$ eV have been performed.

The Debye-Waller factors are calculated from values of $\overline{U}_j^2$ previously measured via LEED.[33] The $\overline{U}_j^2$'s were taken to be 0.0108 Å^2 in the first or surface copper layer and 0.0065 Å^2 in all below-surface Cu layers. The values of $\overline{U}_j^2$ for adsorbed oxygen are estimated to be of the same order as the first substrate layer from prior electron-energy-loss measurements of oxygen adsorbed on Ni (001),[34] so we have tentatively used the value for the first copper layer. However, it is very important to note that the value chosen could be increased by as much as a factor of 4 without significantly affecting calculated anisotropies. This is because $f_j(\theta_j)$ is large only at very low θ_j values for which $W_j \approx 1$ due to the $(1 - \cos\theta_j)$ factor in its argument. Thus, the attenuation of such diffraction anisotropy due to thermal vibration at XPS energies is not expected to be a major effect.

The photoelectron analyzer has a conical acceptance aperture of 3.5° half-angle. In order to approximate the experimental averaging over this, two kinds of nine-point meshes were used to sum the intensities: One consisted of a 4° square on the θ and ϕ axes with points every 2° on both axes and the other was a circle of 2.5° radius with a center point and eight equally spaced points on the periphery. No difference was found between the two schemes of averaging.

Finally, we consider the choice of cluster size in the computation. Since the cluster-size problem for adsorbate overlayer core emission is a special case of that for substrate emission, we consider first the case of substrate core emission for a specific emitter in the nth layer. Note that, for the substrate, intensities must be summed for emission from each type of site and/or layer of atoms. There are then three types of scatterers that can be delineated in relationship to such an emitter. Type (1) is a scatterer in some plane above the emitter such that the scattering angle θ_j can be very small, thus pro-

ducing strong scattering intensities. For the example case of copper, it turns out that for an emitter in the 12th layer, scattering by the first layer atoms produces a maximum scattered intensity of ~5% of the primary intensity (which is the same for all emitters) for $\theta = 45°$. Inelastic attenuation is included in this estimate. The analogous 5% cutoff for an emitter takes place in the fifth layer for $\theta = 7°$. Even with emitters below the 12th layer at $\theta = 45°$, the scattered intensities could be strong since they are amplified by strong forward peaking by neighboring scatterers (and then attenuated by inelastic scattering). Intensities produced by emission from such deep layers $\gtrsim$5% cutoff can be treated to a good approximation as a geometric summation, as for example,

$$I(12) + I(13) + I(14) + \cdots = I(12)(1 + r + r^2 + \cdots)$$
$$= I(12)r/(1 - r),$$

where $I(12)$ is the intensity from the 12th-layer emitter as scattered by all the atoms above the emitter, $r = \exp(-d/\Lambda_e \sin\theta)$, and d is the interlayer spacing. This method of summing for deep layers has been used in our substrate calculations. For adsorbate emission, a type-(1) scatter is not the usual case, as it would imply an emission angle of $\theta \approx 0°$. Type (2) is a scatterer at the same depth below the surface as the emitter, so that the scattering angle θ_j is equal to θ. This type of scatterer is quite important for adsorbate emission. For the same cutoff criterion of 5% of the primary intensity, atoms at 25 Å away along the first layer should be included for Cu. This is probably a conservative choice, however, as it was found that this could be cut down to ~13 Å without any essential changes in predicted anisotropies. For adsorbate emission, this type of scatterer is usually the other adsorbates and in general it is found that this dimension can be cut down to only the first and second nearest-neighbor adsorbates since the scattering power of light atoms like oxygen is weak. Therefore, such adsorbate anisotropies in XPS are expected to require only short-range order for their observation, by contrast with the case in LEED. A type-(3) scatterer lies below the emitter level. In practice, this type turns out generally to give little contribution to calculated anisotropies because only rather weak back scattering would be involved. For grazing-angle emission, however, type-(3) emitters can be important enough to include. Thus, we have finally included several neighbor atoms in the next layer below the emitter in computations for substrate emission, but for adsorbate emission, substrate atoms in the second layer below the surface have little effect on the anisotropy. The final cluster for any calculation was spread over about 90° in azimuth so as to encompass one of eight symmetry-equivalent 45° segments of the (001) surface. After numerous test calculations, 30 oxygen atoms and 90 Cu atoms were included in our calculations for adsorbate emission, whereas approximately 1500 Cu atoms were explicitly summed over in substrate emission.

IV. EXPERIMENTAL RESULTS

Figure 4 shows polar plots of the azimuthal dependence of the O 1s-core photoelectron intensities in $c(2\times2)$ oxygen at polar angles from 7° to 45°, as reported previously.[7] The broken lines are raw data and the solid lines are plots in which the intensities have been averaged over the symmetry-equivalent azimuthal angles of ϕ, $\phi + 90°$, $\phi + 180°$, and $\phi + 270°$ (fourfold average) and minimum intensities have been subtracted off. The

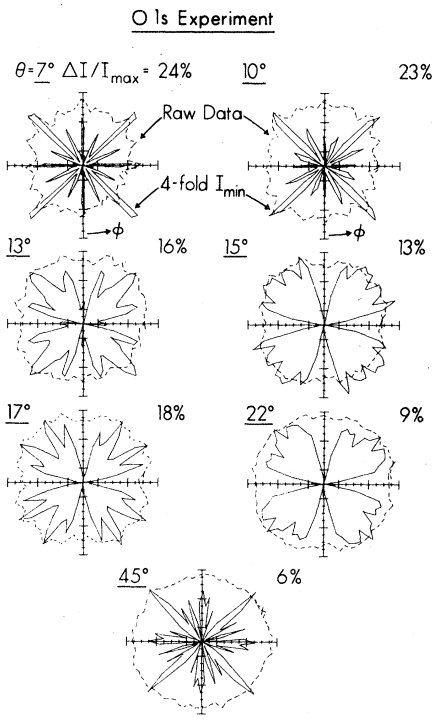

FIG. 4. Azimuthal dependences of O 1s core photoelectron intensities for $c(2\times2)$ oxygen on Cu (001) at polar angles from 7° to 45°. Intensities are proportional to radial distances from the origin in the polar plots. The raw data, over somewhat greater than 360°, are shown dotted. The solid curves represent intensities with fourfold averaging and minimum subtraction. Both the raw and the fourfold-averaged curves are normalized at the highest intensities. The overall degree of anisotropy in the fourfold-averaged data, as given by $\Delta I/I_{max} = I_{max} - I_{min})/I_{max}$, is stated in percentages for each polar angle.

fourfold average is in accordance with the symmetry expected of any pattern arising in the (001) surface or the oxygen overlayer and thus tends only to reduce spurious sources of the intensity variations in the experimental data. The subtraction of minimum intensity magnifies the anisotropy so that it is easier to correlate structure in these "flower patterns" with the raw data. It should also be noted that the mirror-plane symmetry of the (001) surface and the $c(2\times2)$ overlayer structure across directions such as [110] at $\phi=45°$ have not been included in the fourfold averaging; thus the degree of agreement across these mirror planes can be used to estimate the overall reproducibility and accuracy of the measurements. The fine structure found in the averaged curves can also be seen in the raw data for $\theta=7°$, 10°, 13°, and 17°, thus demonstrating a high degree of reliability in the features for those polar angles. The degree of anisotropy is defined as $\Delta I/I_{max}=(I_{max}-I_{min})/I_{max}$ and its values are reasonably high for these cases, as shown by the percentage values given on the figure, which are between 13% and 24%. The four-peak fine structure in the averaged curve for $\theta=15°$ between $\phi=15°$ and 75° is so subtle in the raw curve that the reliability of the fine structure is low. However, taken in the context of curves from $\theta=13°$ to 15° to 17°, there is a clear trend of structure change in which a maximum at $\phi=45°$ for $\theta=13°$ becomes a minimum for $\theta=17°$. This, together with the mirror-plane symmetry of this four-peak structure, further supports the reliability of even the rather subtle features at $\theta=15°$. The three-peak fine structure between $\phi=15°$ and 75° for $\theta=22°$ is not extremely reliable and the anisotropy $\Delta I/I_{max}=9\%$ is now close to the experimental uncertainty; however, the presence of a minimum along $\phi=0°$ can definitely be observed, and a degree of mirror symmetry is found in the three-peak structure. There is no reliable correspondence for $\theta=45°$ between the averaged and the raw data and the very small anisotropy of 6% is less than the experimental uncertainty. Thus more refined measurements will be necessary to obtain sufficiently reliable data for $\theta>22°$.

In order to present the structures in the averaged curves in a more concise way and to make comparisons with theory easier later on, the

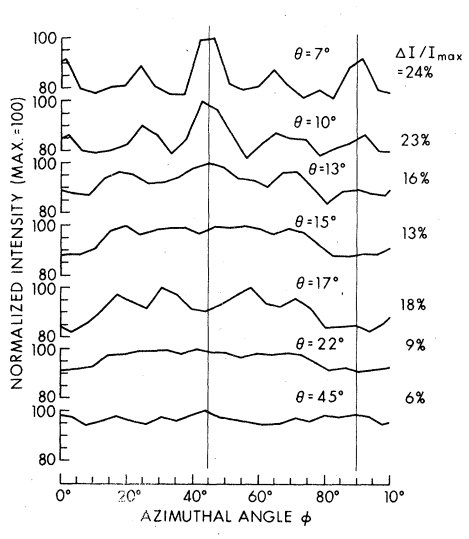

FIG. 5. As in Fig. 4 for the fourfold-averaged data, but plotted in Cartesian coordinates. Note the degree of mirror symmetry of the figures about the azimuth at 45°.

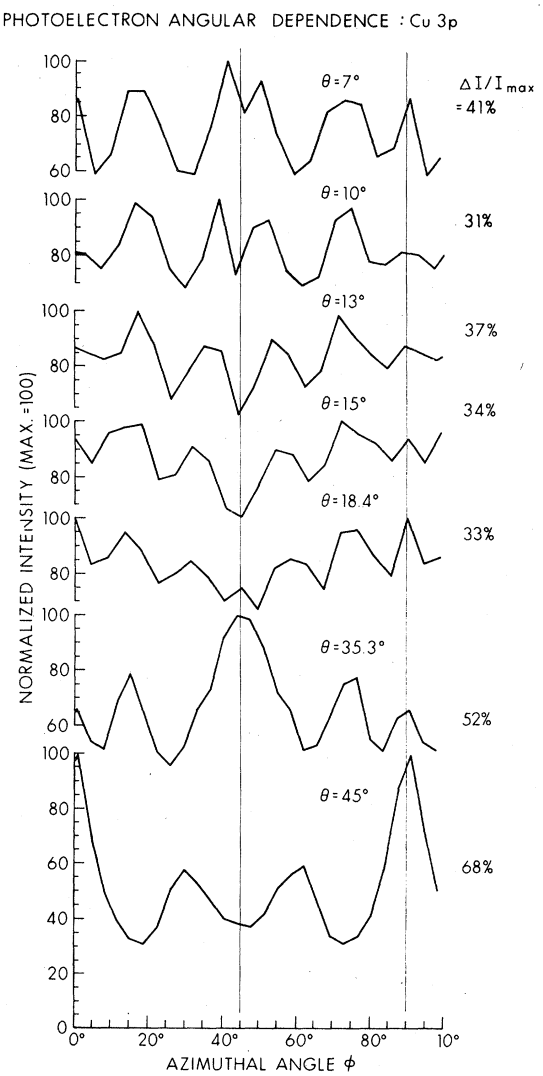

FIG. 6. As Fig. 5, but for the fourfold-averaged azimuthal dependences of Cu 3p-core photoelectron intensities from clean Cu (001) at polar angles from 7° to 45°.

fourfold-averaged data are plotted in a Cartesian manner in Fig. 5. The intensities in the ordinate are normalized to 100 so that $\Delta I/I_{max}$ is the range for each spectrum. The mirror-plane symmetry of the (001) surface and overlayer is consistent with the data in that all reliable structures are symmetric about the azimuth $\phi = 45°$.

Turning now to the anisotropies resulting from substrate emission, we present, in Figs. 6 and 7, Cartesian plots of the fourfold-averaged azimuthal dependences of photoelectron intensities from Cu $3p$ and Cu $2p_{3/2}$, respectively, for a *clean* Cu (001) surface at polar angles in the range $7° \leq \theta \leq 45°$. The general level of the anisotropies in the Cu core emission is significantly higher than for O $1s$, ranging from ~30% for low θ to as high as 70% for $\theta = 45°$. This is natural since the emitters in these cases are not only at the surface but also in the bulk so that very strong forward scatterings can directly contribute to the anisotropy for emitters below the surface. The scattered intensity is furthermore expected to be much stronger for high θ due to the chains of atoms that lie along various low index directions. For instance, the direction at $\phi = 0°$ and $\theta = 45°$ along which very strong peaks are found corresponds to a [110] direction. In fact, several of the polar angles have been chosen specifically to pass through low index directions: $\theta = 18.4° - \langle 310 \rangle$, $26.6° - \langle 210 \rangle$, $35.3° - \langle 111 \rangle$, and $45° - \langle 110 \rangle$. Such pronounced angular dependences of the photoemission intensities from metal substrates have been reported previously for $4d$, $4f$, and valence levels in Au (001),[11] but no detailed theoretical analysis of such effects has been attempted previously. We note further here that there are essential differences in the azimuthal structures between Cu $3p$ and Cu $2p_{3/2}$ for example, at $\theta = 18.4°$ and 45° (no measurement was made of Cu $3p$ at $\theta = 26.6°$). This suggests the importance of interference effects in the superposition of the primary and the scattered waves.

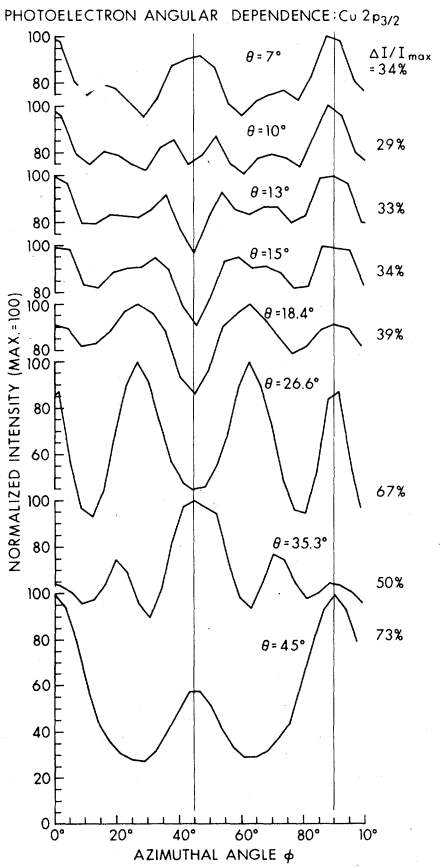

FIG. 7. As Fig. 6, but for Cu $2p_{3/2}$ emission from clean Cu (001).

In order to assess the possible influence of chemisorption on substrate anisotropies, azimuthal scans for Cu $3p$ and Cu $2p_{3/2}$ were also carried out in the presence of a $c(2\times2)$ oxygen overlayer on Cu (001) at the most surface-sensitive polar angle of 7°. These results, however, showed no noticeable differences in comparison with those of the clean surface, and we conclude that the overall weakness of oxygen as a scatterer prevents modification of the strong anisotropies produced by bulk copper scattering.

V. COMPARISON OF THEORETICAL RESULTS WITH EXPERIMENT

We begin this section which compares single-scattering theory and experiment by considering substrate emission, since the metal surface geometry is known and these results thus permit a test of the validity of such a simple model. We then turn to the application of the theory to oxygen adsorbate emission.

A. Substrate core emission at low polar angles

The low polar angles considered here are $7° \leq \theta \lesssim 20°$, where we do not have contributions from large numbers of atoms in chains which produce strong scattering intensities and also perhaps lead to a higher probability of significant multiple-scattering effects. Therefore one would expect better agreement of the SSC calculations with experiment in comparison to the case of higher polar angles of $\theta \gtrsim 20°$. As this is also the range where the adsorbate oxygen core emission shows significant anisotropies, the applicability of the SSC model to this case can thus be tested. In Figs. 8 and 9, the results of the SSC calculations are shown with experiment for Cu $3p$ and Cu $2p_{3/2}$, respectively. The calculations were carried out

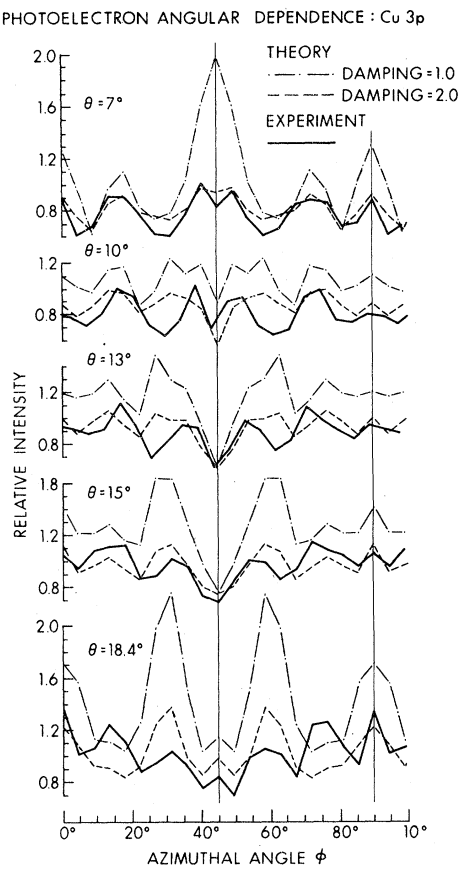

FIG. 8. Comparison of single-scattering cluster calculations with experiment for the azimuthal dependences of photoelectron intensities from the Cu $3p$ core level in Cu (001) for the lower polar angles of $7° \leq \theta \leq 18.4°$. The ordinate scales are theoretical intensities as measured relative to the primary unscattered-electron intensity of unity. The experimental curves have been arbitrarily scaled so as to obtain the best comparison with theory, as all of the sources of background intensity in the experiment are impossible to estimate quantitatively. Calculations are shown for both undamped scattering factors ($\beta = 1.0$) and with a damping of $\beta = 2.0$.

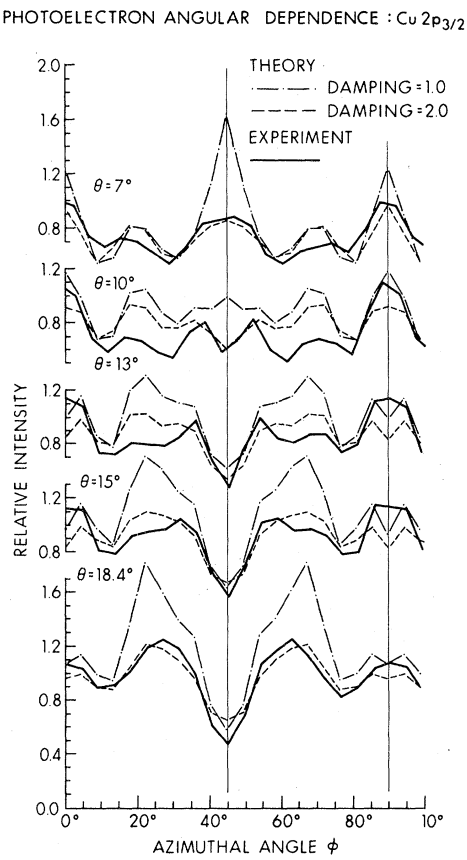

FIG. 9. As in Fig. 8, but for emission from the Cu $2p_{3/2}$ core level.

with the input parameters mentioned in Sec. III C, with full refraction at the surface and with a constant bulk lattice parameter for copper. Although prior LEED studies on clean Cu (001) have reached the conclusion that the deviation of the distance between the first and the second layers from that of the bulk is not more than 5%,[15,16] our model calculations were not at all sensitive to a deviation of this magnitude, even at the most surface-sensitive polar angle of 7°. This is simply because the depth of the emitters contributing significantly to the intensities is too large (~5 layers at $\theta = 7°$) to be sensitive to the first layer contractions. The scattering factors used were with no damping ($\beta = 1.0$) and with an empirically selected value of $\beta = 2.0$ to simulate the effect of certain other effects not included in the theory, as mentioned in Sec. III C.

We begin by discussing the theoretical results with no damping. As far as peak *positions* are concerned, the agreement between theory and experiment is very good, although there are a few exceptions. The exceptions appear for Cu $3p$ at (1) $\theta = 7°$ and $\phi \approx 45°$, (2) $\theta = 10°$ and $\phi \approx 35°$, (3) $\theta = 13°$ and $\phi \approx 30°$, and for Cu $2p_{3/2}$ at (4) $\theta = 10°$ and $\phi \approx 45°$. These exceptions are such that theory shows a broad single peak where two partially resolved peaks are found in the experiments for (1) and (4), and that theory shows a broader and more complex peak where a single peak is found in the experiments for (2) and (3). It is also obvious that the relative peak intensities in the theory are not in particularly good agreement with experiment. For example, peaks at $\theta = 7°$ and $\phi \approx 45°$ for Cu $3p$ and Cu $2p_{3/2}$ are too strong in the theory. The case at $\theta = 18.4°$ for Cu $3p$ shows the worst agreement as to relative peak intensities, even though all peak positions (including a weak feature in theory at $\phi \approx 15°$) are well pre-

TABLE I. Theoretical and experimental azimuthal anisotropies of photoelectron intensities, defined as $\Delta I/I_{max}$. Emission is from the Cu $3p$ and Cu $2p_{3/2}$ core levels of a clean Cu (001) surface at polar angles of $7°\leq\theta\leq45°$, and calculations have been performed with and without damping factors for the elastic scattering ($\beta=1.0$ and 2.0, respectively). The numbers in parentheses for $\beta=1.0$ are for a cluster approximately one-half as large in number of atoms.

		Cu $3p$						Cu $2p_{3/2}$						
	θ	7°	10°	13°	15°	18.4°	35.3°	45°	7°	10°	13°	15°	18.4°	26.6°	35.3°	45°
$\Delta I/I_{max}$	Experiment	0.41	0.31	0.37	0.34	0.33	0.52	0.68	0.34	0.29	0.33	0.34	0.39	0.67	0.50	0.73
	$\beta=1.0$	0.69	0.28	0.51	0.58	0.51	0.44	0.87	0.67	0.43	0.53	0.65	0.68	0.54	0.62	0.77
		(0.64)	(0.39)	(0.56)	(0.58)	(0.60)			(0.68)	(0.53)	(0.56)	(0.64)	(0.73)			
	$\beta=2.0$	0.37	0.42	0.42	0.32	0.41	0.32	0.76	0.43	0.34	0.48	0.48	0.46	0.45	0.38	0.62

dicted. It should be emphasized as an overall comment, however, that the peak positions in theory in general reproduce very well the trends shown by both the Cu $3p$ and $2p_{3/2}$ experimental data. Another type of discrepancy between the undamped theory and experiment is the degree of anisotropy, defined as $\Delta I/I_{max}$. These values are tabulated in Table I, and it is clear that undamped theory predicts ~1.5–2.0 times too much anisotropy for almost all cases. To investigate whether cluster size is related to this discrepancy, the values in parentheses for $\beta=1.0$ are those for theory with a smaller cluster of ~$\frac{1}{2}$ the surface area of the optimized or converged cluster. The values with the smaller cluster show in general only a slight increase over the converged cluster, and there was no essential change in the azimuthal pattern with the size of the cluster, suggesting the sufficiency of our cluster size.

As described in Sec. III, there are at least five possible causes for the disagreement as to relative peak intensity or degree of anisotropy, and the inclusion of a damping factor in $f_j(\theta_j)$ may provide a crude approximation for allowing for the effects. Thus we have investigated various damping factors to determine whether they improve the agreement or not. $\beta=2.0$ is found to be the value for which the best agreement is reached for all the cases. The theoretical curves with $\beta=2.0$ in Figs. 8 and 9 in fact show substantial improvement of relative peak intensities in comparison with experiments, but with no effects on the peak positions, which were already in good general agreement at $\beta=1.0$. The anisotropies $\Delta I/I_{max}$ with $\beta=2.0$ listed in Table I also show substantial improvement in comparison to experiment. Note also that the previously discussed discrepancies (1) and (4) are both markedly reduced by this damping of β. These results therefore suggest that the net effect of anisotropic inelastic scattering and certain other phenomena not included in this theory can be crudely approximated, within the framework of the single-scattering model, by damping of $f_j(\theta_j)$, and further that the net effect is not likely to be a change in peak positions but rather only in intensities.

B. Substrate core emission at high polar angles

We now consider the higher polar angles of $20°\leq\theta\leq45°$. Figures 10 and 11 show the comparison of theory with experiment. The undamped theory with $\beta=1.0$ shows good agreement with experiment as to peak positions and follows the general trends of the experimental data with θ. Note especially, that the overall fine structure observed is very well predicted for Cu $3p$ at $\theta=45°$, and $2p_{3/2}$ at $\theta=26.6°$ and 45°. On the

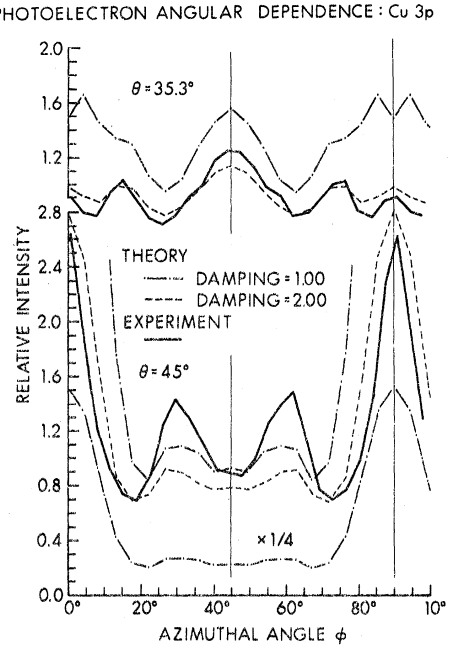

FIG. 10. As in Fig. 8, but for emission from Cu $3p$ at the high polar angles of $20° \lesssim \theta \leqslant 45°$.

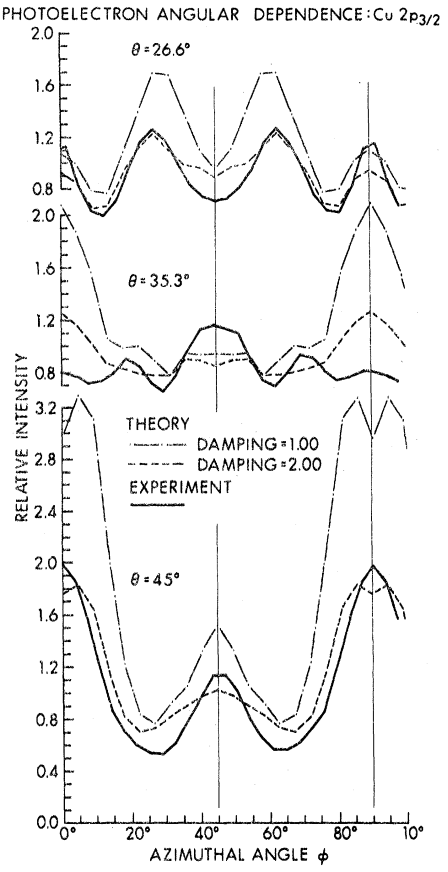

FIG. 11. As in Fig. 8, but for emission from Cu $2p_{3/2}$ at the high polar angles of $20° \lesssim \theta \leqslant 45°$.

other hand, there are a few substantial discrepancies between theory and experiment as to relative peak intensities and fine structure. For example, the $\beta = 1.0$ theory for Cu $3p$ at $\theta = 35.3°$ shows an inverted intensity relationship as compared to the experiment and a doublet at $\phi = 0°$–$10°$ compared to the singlet observed. A similar type of intensity inversion is found for Cu $2p_{3/2}$ at $\theta = 35.3°$. On the other hand, the theoretical anisotropies $\Delta I/I_{max}$ with $\beta = 1.0$ show values comparable to experiment except for the case of Cu, $3p$ at $\theta = 45°$, as listed in Table I. The inclusion of the $\beta = 2.0$ damping in $f_j(\theta_j)$ is helpful for Cu $3p$ (see especially curves for $\theta = 35.3°$) and also Cu $2p_{3/2}$, but to a lesser degree for the latter. Even with $\beta = 2.0$, Cu $2p_{3/2}$ at $\theta = 35.3°$ does not yield intensity relationships very close to experiment. The anisotropies $\Delta I/I_{max}$ for theory with $\beta = 2.0$ also show even lower values as compared to experiment, as listed in Table I. This seems to demonstrate that, although general agreement as to peak positions is obtained, the level of agreement of the SSC calculation for high polar angles is not as good as that for low polar angles, even with an empirical adjustment of β.

C. Adsorbate core emission

The bonding geometry of $c(2\times2)$O on Cu (001) is not known for certain.[15,16] The two most plausible geometries for oxygen proposed on the basis of prior LEED studies are a coordination in fourfold hollows or a reconstruction with O atoms replacing every other Cu atom in the (001) surface.[15,16] Also, two domains of twofold bridge sites 1.5 Å above the surface and at right angles to one another have been tentatively suggested.[35] Within any of these choices, the position z of the O atoms along the surface normal with respect to the first-layer Cu-atom centers constitutes the only geometric variable. Thus, theoretical calculations of O $1s$ intensities have been performed for the full range of physically reasonable z positions in both the fourfold and reconstructed geometries ($-0.2 \leqslant z \leqslant 1.5$ Å for fourfold hollow and $-1.5 \leqslant z \leqslant 1.5$ Å for reconstructed), as well as for the value $z = 1.5$ Å suggested by LEED for the twofold site. The calculations performed with damping factors $\beta = 1.0$ and $\beta = 2.0$ showed identical peak positions in the azimuthal anisotropies, but some improvements in relative peak intensities for $\beta = 2.0$, in the same manner as the results for substrate core emission at low polar angles. The only geometry for which all major peaks and minima over the range $7° \leqslant \theta \leqslant 17°$ are

correctly predicted in the theoretical curves for either $\beta=1.0$ or 2.0 is fourfold-hollow coordination in which the O atoms are coplanar with the Cu atoms (i.e., $z=0.0$ Å). No agreement is found for the twofold site at $z=1.5$ Å. We further note here that there has been a very recent suggestion based upon an analysis of secondary-ion mass-spectrometry data by Holland *et al.*[36] that the oxygen atom is present in a fourfold-hollow site somewhere between $z=1.2$ and 1.5 Å above the Cu (001) plane. Comparison of our SSC calculations with experiment for those geometries does not indicate agreement, so that it is not a likely geometry from our viewpoint. The azimuthal anisotropies calculated for several z positions of the fourfold site and the optimum z position of the reconstructed site are shown in Figs. 12–16, together with the experimental results. The theoretical results for the fourfold-hollow geometry are shown with five z values (0.0, ±0.1, and ±0.2 Å) to demonstrate the sensitivity of the anisotropy to the z positions. The theoretical curves for the fourfold-hollow sites at $z=0.0\pm0.1$ Å agree very well with experiment for almost all polar angles, with the highest degree of agreement at $z=0.0$ Å. The theoretical curves for $z=\pm0.2$ Å show obvious deviations from the experimental curves, thus indicating a sensitivity of the geometry determination of ~±0.1 Å for the case in question. The theoretical curves for the optimum geometry in the reconstructed structure show reasonable agreement with experiment at $\theta=7°$ and 10° but do not agree well for $\theta=13°$–17°. There-

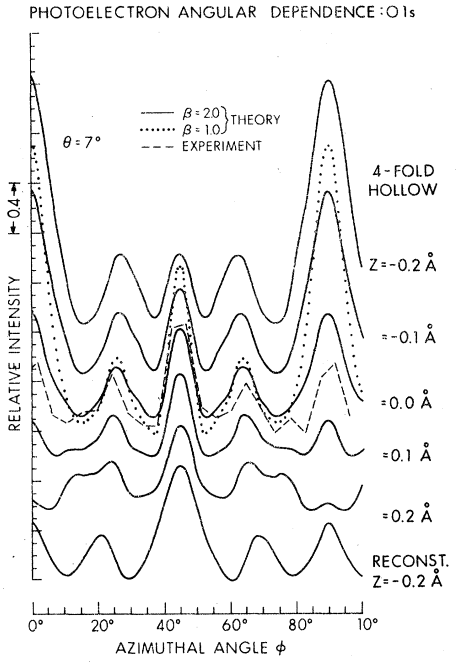

FIG. 12. Comparison of single-scattering cluster calculations with experiment for the azimuthal dependence of photoelectron intensities from the O 1s core level in $c(2\times2)$ oxygen on Cu (001) at a polar angle θ of 7°. The ordinate scales are theoretical intensities relative to the primary electron intensity of unity. The dotted line is a theoretical curve with $\beta=1.0$ for oxygen in a fourfold-hollow site at $z=0.0$ Å. The dashed experimental curve is arbitrarily scaled so as to obtain the best comparison with theory at $z=0.0$ Å. The solid curves are for $\beta=2.0$ and are given for several z values with fourfold coordination and the empirically optimum z value for a reconstructed geometry.

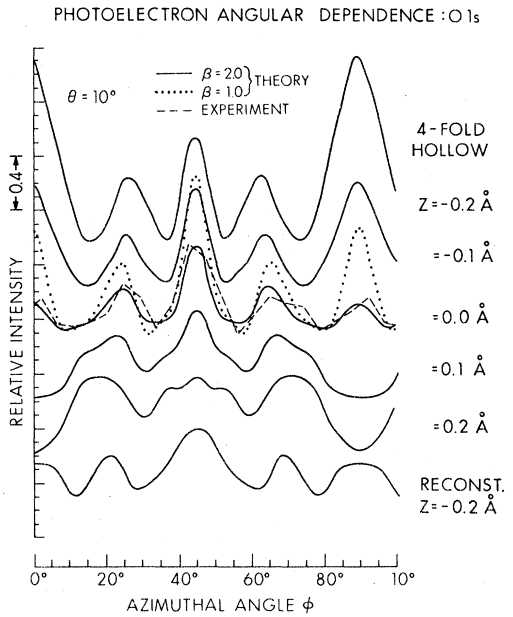

FIG. 13. As in Fig. 12, but for a polar angle of 10°.

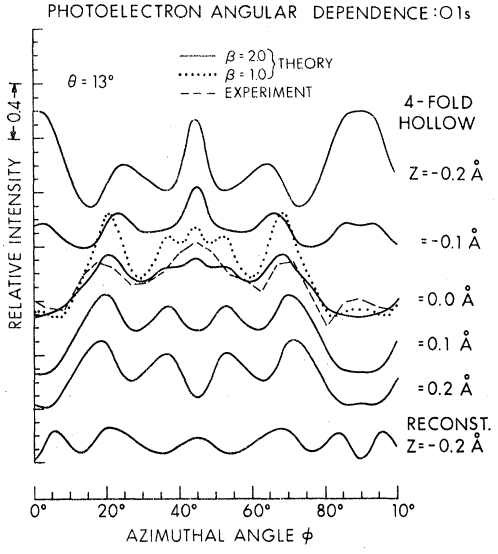

FIG. 14. As in Fig. 12, but for a polar angle of 13°.

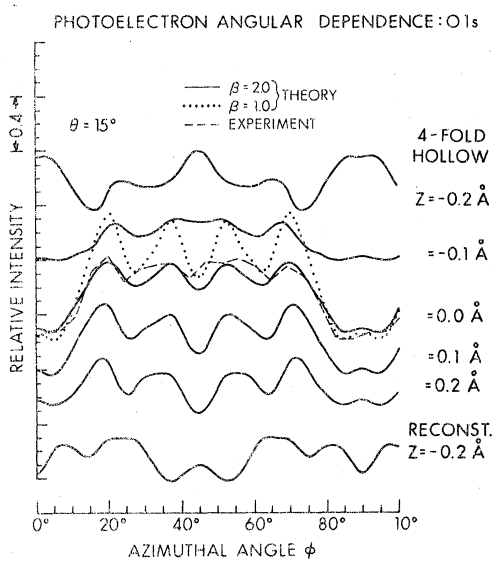

FIG. 15. As in Fig. 12, but for a polar angle of 15°.

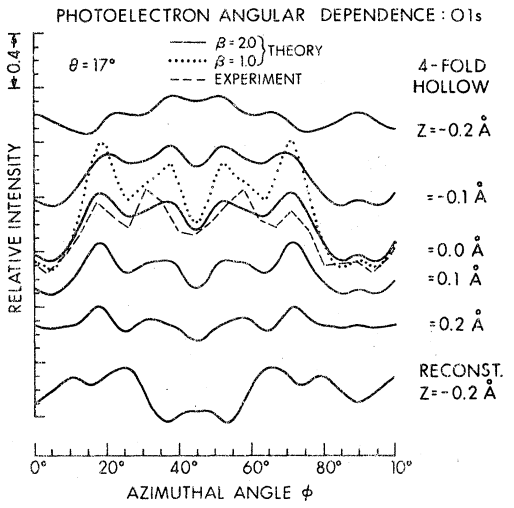

FIG. 16. As in Fig. 12, but for a polar angle of 17°.

fore these calculations strongly suggest the fourfold-hollow site at $z = 0.0 \pm 0.1$ Å for $c(2\times2)$ oxygen on Cu (001).

Examining the results further, we see again from Table II that there is considerable disagreement between theory and experiment as to $\Delta I/I_{max}$ even for the case $\beta = 2.0$, even though the relative peak intensities are well predicted by theory with $\beta = 2.0$, as can be seen in Figs. 12–16. The experimental anisotropies are obviously lower than those of theory by factors of as much as 3.5–4.0. This type of disagreement was not as serious for substrate core emission at low polar angles. One of the most plausible causes for this is multiple bonding sites perhaps associated with a certain amount of imperfection in the $c(2\times2)$ oxygen overlayer, as is perhaps indicated by the rather diffuse and weak $c(2\times2)$ LEED spots. In that case the oxygen atoms in the nonideal positions may produce a uniform-background intensity in the azimuthal pattern, or at least some sort of averaging in it, thereby decreasing the observed anisotropy $\Delta I/I_{max}$.

The accuracy of the present geometry determination with this model is not much affected by the uncertainty in the true amount of electron refraction occurring at the surface. The results at the extreme limit of no refraction ($V_0 = 0.0$ eV) are easily estimated by replacing the polar angles for the theory in Table II by the angles in brackets which are the polar angles inside the solid. Then a rough comparison between theory for this case and experiment can be done by taking the theoretical curves one step lower in polar angle. Comparisons made in this way tend to move the optimum z-position range only from −0.1 to 0.1 Å to about 0.0 to +0.2 Å. However, we in any case predict oxygen to lie well down below the surface of the copper charge density and also the change in the inner potential by oxygen adsorption should

TABLE II. As in Table I, but for emission from the O 1s core level in $c(2\times2)$ oxygen on Cu (001) at polar angles of $7° \leq \theta \leq 17°$. The oxygens are either in a fourfold hole and coplanar with the Cu surface atoms ($z = 0.0$ Å), or in a reconstructed surface at $z = -0.2$ Å. The internal emission angles before refraction are given in parentheses.

	θ	7° (9.9°)	10° (12.2°)	13° (14.7°)	15° (16.5°)	17° (18.3°)
$\Delta I/I_{max}$	Experimental	0.24	0.23	0.16	0.13	0.18
	Fourfold $\beta = 1.0$	0.85	0.62	0.52	0.60	0.57
	Fourfold $\beta = 2.0$	0.62	0.45	0.41	0.44	0.40
	Reconst. $\beta = 1.0$	0.83	0.69	0.40	0.47	0.53
	Reconst. $\beta = 2.0$	0.60	0.42	0.23	0.29	0.34

only be of the order of hundreds of meV.[37] Thus, a very nearly full inner potential should be more correct, and the accuracy of the geometry determination is most likely to remain within $z=0.0 \pm 0.1$ Å.

VI. DISCUSSION

We begin by discussing the physical and chemical plausibility of finding the chemisorbed oxygen atoms coplanar with the first Cu layer in fourfold-hollow sites. The bond lengths between an O atom and its neighboring Cu atoms are in a physically reasonable range: The bond length to the four nearest Cu atoms in the surface layer is 1.81 Å and that to the Cu atom just below the oxygen atom is also 1.81 Å for $z=0.0$ Å. By comparison, the Cu–O bond lengths in some typical compounds of copper and oxygen range from 1.8–2.1 Å (Ref. 38) and Cu_2O has a bond length of 1.84 Å not very much different from the 1.81 Å required by this structure.[38] The stoichiometry of O and Cu in the surface layer is also the same as that in Cu_2O, but with additional bonding to the Cu layer below the surface. Indeed, the additional coordination of having five Cu–O bonds and the difference of bond geometry in chemisorption as compared to four tetrahedral Cu–O bonds in Cu_2O may account for the slight bond-length decrease. Another piece of evidence which qualitatively supports the feasibility of the O geometry is that the ionic state of Cu in the first layer is the same as that in Cu_2O. That this is true was first suggested by Evans[39] in a study of the oxidation of polycrystalline Cu. The XPS spectra for the Cu $2p$ levels showed no shake-up satellite peaks during the early stages of oxidation, and the well-known correlation between the ionic state of Cu and the shake-up satellites thus suggests the existence of $Cu^+ 3d^{10}$ near the surface.[39] Braithwaite *et al.*[14] have reported LEED and XPS measurements of oxygen adsorption on a Cu (001) surface at 80 and 290 K. They found no satellite peaks in the Cu $2p_{3/2}$ level for exposures corresponding to both the "four-spot" and $c(2\times2)$ LEED structures at 80 and 290 K and pointed out these facts as evidence of no surface reconstruction at these stages of adsorption. They further suggested that the stability of $c(2\times2)$ oxygen is associated with the formation of a surface compound of Cu_2O, although their speculative oxygen adatom position is situated somewhat above the copper (001) unreconstructed surface. Hofmann *et al.*[37] reported LEED and work-function measurements on the chemisorption system in question as a function of O_2 exposure at several temperatures above 300 K. In the discussion of the four-spot structure and work-function changes with exposure, they also favored a nonreconstructed structure for $c(2\times2)$ oxygen. Also, in a further discussion of work-function changes at higher exposure corresponding to the $(\sqrt{2}\times2\sqrt{2})$ $R45°$ LEED structure, they proposed an incorporative model which is quite suggestive of the geometry presented in this work for the $c(2\times2)$ $[=(\sqrt{2}\times\sqrt{2})$ $R45°]$ oxygen structure in that oxygens are coplanar with coppers in fourfold holes in various planes at and below the surface (cf. Fig. 5 in Ref. 37). Thus, if an oxygen adatom can sit just at the coplanar center of the fourfold-hollow site in the surface plane, this should also be possible in the hollow sites within the second and subsequent Cu layers, as little change is required in the overall electronic environment of the oxygen and copper atoms. This lack of drastic change in environment is also in agreement with the fact that no satellite peaks are found in Cu $2p_{3/2}$ for the $(\sqrt{2}\times2\sqrt{2})$ $R45°$ structure and that only a 0.3-eV shift of the oxygen $1s$ binding energy was found in XPS spectra in going from the $c(2\times2)$ to $(\sqrt{2}\times2\sqrt{2})$ $R45°$ structure.[14]

The oxygen overlayer position for $c(2\times2)$O on a Cu (001) surface as proposed in this work is in contrast to the position of the same $c(2\times2)$ overlayer on Ni (001). Comprehensive LEED experimental[40] and theoretical[41] studies have reached the relatively firm conclusion of an oxygen position which is in the fourfold-hollow site at a z position of 0.9 Å. This is not in contradiction to the present result, however, since there is a large difference in the nature of chemisorption between Ni and Cu.[42] (See note added in proof.)

Since the adsorbate position proposed in this work is coplanar with the first substrate layer and this may not generally be the case for other adsorbates and substrates, it is worth exploring features of the technique presented here as it might be applied to general chemisorption systems. In Figs. 17(a) and 17(b), we show SSC calculations with several choices of cluster size for oxygen positions of $z=0.0$ and 1.0 Å in a fourfold-hollow site. For a full-size cluster (solid lines), it is obvious that azimuthal anisotropies are much more pronounced for an oxygen position of $z=0.0$ Å than for $z=1.0$ Å. This is merely because forward-peaked scattering, especially from copper, is detected more easily for oxygen positioned at $z=0.0$ Å. Thus, this indicates that chemisorption systems with adsorbates high above the surface layer will not give anisotropies as large in azimuthal scans. In Fig. 17(a), calculations for oxygen at $z=0.0$ Å are shown for a fully converged cluster, a cluster with full-sized substrate only (dashed line) and a cluster whose sub-

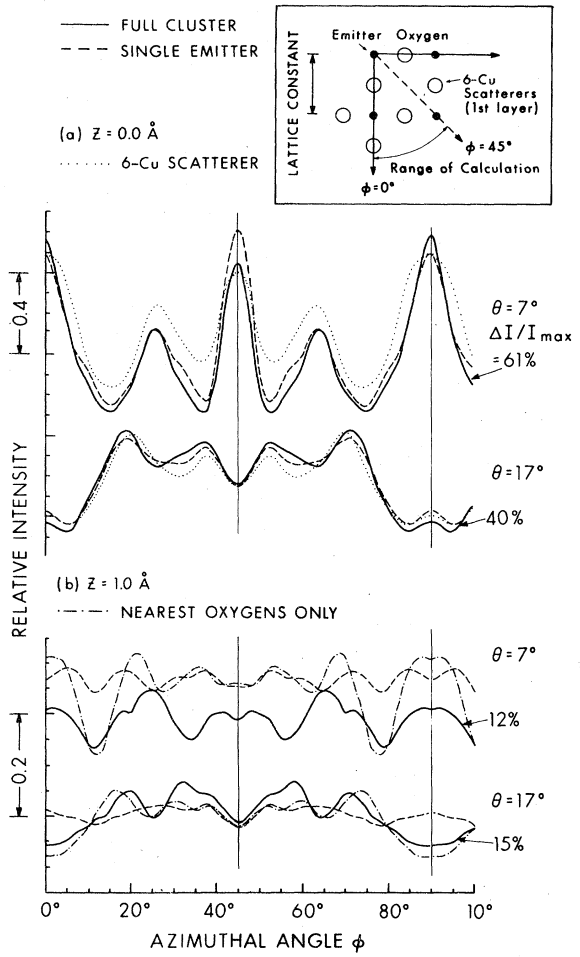

FIG. 17. Single-scattering cluster calculations of the azimuthal dependence of photoelectron intensities from the O 1*s* core level for an oxygen emitter in a fourfold-hollow site on Cu (001) at (a) $z = 0.0$ and (b) $z = 1.0$ Å with several choices of cluster size in the calculations. Calculations were performed with $\beta = 2.0$. Solid lines are calculations with the full cluster of 30 oxygen atoms and 90 copper atoms, as used in Figs. 12–16, and dashed lines are those with a full substrate copper cluster but only a single oxygen atom as an emitter. Dotted lines are calculations for $z = 0.0$ Å with only a six-copper cluster in the surface layer as shown in the inset, and dot-dashed lines are those for $z = 1.0$ Å with a cluster consisting of two first- and one second-nearest-neighbor oxygens, as shown in the inset. The ordinate scales are theoretical intensities relative to the primary electron intensity of unity and they are different for (a) and (b). Arbitrary changes in the ordinate scale between curves for $\theta = 7°$ and 17° are included. The overall anisotropies $\Delta I/I_{max}$ are given for the full cluster curves.

strate is just six neighbor atoms as shown in an inset (dotted line). The differences in the patterns for these calculations are very little; the only substantial change is found in the peak width at $\phi = 90°$ for the six-Cu case. Thus, this indicates that for adsorbates lying well into the surface layer (and most probably, also further below the surface layer) the azimuthal patterns result from forward scattering by only near-neighbor *substrate* atoms. This further suggests the extended usage of this technique for structure studies involving oxidation and ion implantation. In Fig. 17(b), the azimuthal patterns calculated for a full cluster, a cluster with only the first and second nearest-neighbor oxygen and substrate atoms (dashed line) and a single-emitter cluster of only substrate atoms (dashed-dotted lines) are compared for $z = 1.0$ Å. The cluster with near-neighbor oxygens shows about the same result as the full-cluster calculation except for directions of lower θ and $\phi \approx 45°$. However, the calculation for a cluster of only substrate atoms shows drastic change and less anisotropy. This result serves to demonstrate that a great deal of the azimuthal anisotropy for adsorbates at higher positions ($z \gtrsim 1.0$ Å) originates from forward scattering by the near-neighbor adsorbates, and thus that the determination of the chemisorption geometry with respect to the substrate could be somewhat more difficult for those systems. However, it should be noted that information is thus obtained concerning the geometry with respect to other adsorbates, and that scattering within a *molecular* adsorbate, as discussed in Sec. III, can also be used for a determination of the bond-axis orientation of a molecular adsorbate.[28]

We now discuss reasons why such single-scattering calculations might be successful in predicting electron diffraction phenomena for core-level photoemission in the XPS regime. In general, the condition for applicability of a single-scattering model is that the strength of the single scattering be weak enough so that the contribution of multiple scattering to the coherent superposition of single-scattered waves is negligibly weak. It has been pointed out for LEED (Ref. 1) that the strength of the backward scattering that must produce most of the single-scattered intensity is in fact weak (~1% of the primary), but that the strength of the associated forward scattering is not weak and this acts as the source for multiple scattering. Another factor affecting the importance of multiple scattering is the strength of inelastic scattering, which weakens the effective strength of elastic scattering. For example, as a result of this effect, single scattering is in fact valid for the case of LEED experiments on crystalline xenon, as has been reported by Ignatjevs *et al.*[43] In this case, because of the large atomic volume of xenon, the effective elastic-scattering strength per unit volume is weak in comparison to typical metals such as nickel and

copper, leading to excellent agreement between experiment and single-scattering theory.[43] The situation for the present XPS case seems to be different from this. To illustrate this, we first examine the strength of scattering at a typical energy of ~10^3 for atoms and molecules for which experimental values are available. Total elastic-scattering cross sections for rare gases from neon to xenon have been found to decrease by a factor of 3 in going from ~100 to ~1000 eV.[44] For light elements such as nitrogen and oxygen, measurements show about the same degree of decrease in total scattering cross sections with energy.[44] On the other hand, the change in electron mean free path due to inelastic scattering in solids in going from ~100 to ~1000 eV also increases by a factor of 3. Therefore, it is rather likely that the effective scattering strength for the XPS energy regime is not substantially lower than for LEED, since the combined effects of scattering strength and mean free path tend to cancel each other. Thus, the reasons for the empirical validity of single scattering must lie elsewhere. Another characteristic of electron-atom scattering at high energies is the increased sharpness and dominance of forward peaking (cf. Fig. 3). The sharpness can be illustrated by noting typical FWHM's (full-widths at half-maximum intensity) of the forward peak of ~10°–20° for 1000 eV and ~20°–50° for 100 eV.[44] Thus, it is the strong forward scattering that must be responsible for most of the diffraction. Understanding these characteristics of the XPS case, we can thus mention two likely reasons for the utility of single scattering as follows: (1) the effects of multiple scattering may decrease because of the narrower peak width in forward scattering, except for low-index directions where multiple forward scattering might be expected; (2) the forward-scattering intensity also may not be affected much by multiple scattering because of the short-range nature of this scattering (cf. discussion in Sec. II B).

Comparing the present analysis to prior XPS studies of the systematics of core-level anisotropies, we note that Baird *et al.*[11] measured final-state diffraction effects for x-ray photoelectrons from Au 4*d*, 4*f* and valence levels of Au (001), and a Kikuchi-band phenomenology was used qualitatively in their explanation of these effects. Most of the major features in the intensity distribution could be approximately explained as a superposition of Kikuchi bands associated with various low-index planes. However, the kinetic energies of the photoelectrons from Au 4*d*, 4*f* and valence levels in this case were rather close to each other (1140–1480 eV), so that the differences in any diffraction features due to the electron kinetic energy would not be obvious, and that is consistent with these earlier data. In the present study, as mentioned in Sec. IV, the diffraction features in Cu 3*p* and Cu $2p_{3/2}$ photoelectrons (where the kinetic energies are 1420 and 563 eV, respectively) differ substantially in certain cases, indicating the importance of interference effects in the scattering. A more recent analysis by Goldberg *et al.*[45] using Kikuchi-band superposition in a more quantitative way does, however, show a reasonable degree of agreement between theory and experiment for the high-angle Cu data presented here. However, the SSC calculations exhibit better agreement and are, from first principles, a more accurate way of including all single-scattering effects. Thus, the Kikuchi-band approach appears limited to a zeroth-order phenomenological description that could be qualitatively useful in certain instances.

We turn now to a brief discussion of the general relationship of this work to prior studies aimed at determining surface structures by various forms of electron diffraction. There have been two recent reports of photoemission measurements of adsorbate core levels which are very closely related to the present work. Woodruff *et al.* and Norman *et al.*[9] have reported the angular dependence of Te 4*d*, Na 2*p*, and Se 3*d* core-level photoemission for those atoms adsorbed on Ni (001) with excitation energies of ~80–100 eV and at rather high polar angles of ~30°–60°. The fact that a large degree of angular dependence arises at these high polar angles can be understood in terms of the behavior of $f_j(\theta_j)$ at low energies, because it can have reasonable high values at large scattering angles for primary electron energies of ~50–100 eV.[22] The photoelectron kinetic energies involved in this experiment also correspond to those of LEED in which large-angle scattering is clearly observed. However, working at such low energies also implies the necessity of full multiple-scattering calculations with input parameters of the same level of reliability as LEED calculations.[9] Also, Kevan *et al.*[10] have recently measured photoelectron diffraction effects for the Se 3*d* level in a Se overlayer on Ni (001) for emission along the surface normal as a function of incident photon energy between 30 and 190 eV. Thus, final electron energy is changed rather than angle, and this is a complementary method to the techniques reported here and in Ref. 9. However, the incident energies utilized again require calculations at the same level of complexity as LEED.

The use of MEED (medium-energy-electron diffraction) has also been proposed by Moon and Cowley[46] as a complementary technique to LEED and RHEED (reflective high-energy electron diffrac-

tion). In this method, incident electron beams of medium energy (1–10 keV) are used at grazing incidence and exit angles. In view of the success of single-scattering calculations for the analysis of our angle-resolved XPS results, similar kinematical calculations for the interpretation of MEED may be sufficient, although the sensitivity of MEED to adsorbate geometry may not be as high as in the present measurements. It should, however, be noted that there have also been important advances in the theory of angle-resolved electron emission from substrate core levels in the energy range of 10^2-10^3 eV, as, for example, the chain method of Lindsay and Pendry.[47] As we have noted that the SSC calculations do not show as high a level of agreement with experiment for substrate core emission at high polar angles, it thus may be necessary to consider a more detailed theory including dynamical effects for certain cases. However, comparing the limited number of theoretical curves so far obtained with the chain method for Cu $2s_{1/2}$ and Cu $2p_{3/2}$ emission at $\theta = 35.3°$ (Ref. 47) with experimental data does not show a significantly better degree of agreement than with the SSC results.

In summary, we point out a few advantages and a disadvantage of such angle-resolved XPS studies of adsorbate core levels as follows: (1) A reasonably accurate analysis appears possible in terms of single-scattering theory, as we have shown in this work. Furthermore, the final results are not particularly sensitive to the exact choices of scattering factors, electron attenuation lengths, the degree of atomic vibration, and the value of the inner potential. (2) Nonordered or very dilute chemisorption systems can be examined, especially for systems with adsorbates located well below the surface, which is a large advantage over LEED. (3) Intramolecular scattering effects can be used for the determination of admolecule orientation, as mentioned briefly in Sec. III, and discussed more recently by Petersson *et al.*[28] (4) As a possible disadvantage, diffraction effects for core emission from a low-z adsorbate located well above the first substrate layer are expected to be weak because of the difficulty of achieving low substrate scattering angles in emission. Thus, anisotropies may tend to be much weaker for such cases, and analyses correspondingly more difficult.

VII. CONCLUSIONS

It has been demonstrated that final-state diffraction in core-level x-ray photoemission from $c(2\times2)$ oxygen on Cu (001) is strong enough to be detected at low electron take-off angles. The applicability of a simple single-scattering cluster model for describing such effects has been confirmed by comparing experiment and theory for substrate core-level x-ray photoemission. For adsorbate emission, very good agreement has been found between experiment and theory for oxygen adsorbed in a fourfold-hollow site at a vertical position coplanar with the first Cu layer. The general application of this technique to the determination of chemisorption geometries thus seems possible, particularly with additional refinements in experimental and theoretical methodology.

Note added in proof. Recent XPS work in our laboratory [L. G. Petersson *et al.*, Mater. Sci. Eng. 42, 111 (1980)] in fact suggests that $c(2\times2)$ O on Ni $\overline{(001)}$ may consist of a mixture of above-plane and in-plane adsorption sites.

ACKNOWLEDGMENTS

We are indebted to J. B. Pendry for providing us with phase shifts and Z. Hussain for preparing the single crystals. The support of the National Science Foundation (Grant No. CHE76-24506) and the Petroleum Research Fund of the American Chemical Society is also gratefully acknowledged. One of use (C.S.F.) also gratefully acknowledges the support of the Laboratory for the Utilization of Electromagnetic Radiation (L.U.R.E) and the University of Paris during a portion of this work.

*Present address: Dept. of Physics, Faculty of Science, Tohokn University, Sendai, 980 Japan.

†Present address: Stanford Synchrotron Radiation Laboratory, Stanford, California 94305.

‡Address during 1978–79: L.U.R.E., C.N.R.S. et Université de Paris Sud, 91405 Orsay, France. Present address: Department of Chemistry, University of Utah, Salt Lake City, Utah 84112.

[1]See, for example, J. B. Pendry, *Low Energy Electron Diffraction* (Academic, London, 1974).

[2]J. A. Strozier, Jr., D. W. Jepsen, and F. Jona in *Surface Physics of Materials*, edited by J. M. Blakely (Academic, New York, 1975), Vol. 1.

[3]See, for example, C. H. Li and S. Y. Tong, Phys. Rev. Lett. 40, 46 (1978) and references therein.

[4]See, for example, E. A. Stern, D. E. Sayers, J. G. Dash, H. Shecher, and B. Bunker, Phys. Rev. Lett. 38, 767 (1977); P. H. Citrin, P. Eisenberger, and R. C. Hewitt, *ibid.* 41, 309 (1978), and references therein.

[5]See, for example, F. W. Saris and J. F. van der Veen, *Proceedings of the 7th International Vacuum Congress and 3rd International Conference on Solid Surfaces, Vienna, 1977* (IVC, ICSS, Vienna, 1977), Vol. III, p.

2503, and references therein.
[6]S. Kono, C. S. Fadley, N. F. T. Hall, and Z. Hussain, Phys. Rev. Lett. 41, 117 (1978).
[7]S. Kono, S. M. Goldberg, N. F. T. Hall, and C. S. Fadley, Phys. Rev. Lett. 41, 1831 (1978).
[8]A. Liebsch, Phys. Rev. Lett. 32, 1203 (1974); Phys. Rev. B 13, 544 (1976).
[9]D. P. Woodruff, D. Norman, B. W. Holland, N. V. Smith, H. H. Farrell, and M. M. Traum, Phys. Rev. Lett. 41, 1130 (1978); D. Norman, H. H. Farrell, M. M. Traum, R. P. Merrill, and T. N. Rhodin, in Proceedings of the 2nd European Conference on Surface Science, Cambridge, 1979 (unpublished).
[10]S. O. Kevan, D. H. Rosenblatt, D. Penlay, B. C. Lu, and D. A. Shirley, Phys. Rev. Lett. 41, 1565 (1978).
[11]R. J. Baird, C. S. Fadley, and L. F. Wagner, Phys. Rev. B 15, 666 (1977) and references therein.
[12]R. J. Baird and C. S. Fadley, J. Electron Spectros. Relat. Phenom. 11, 39 (1977).
[13]L. McDonnell and D. P. Woodruff, Surf. Sci. 46, 505 (1974).
[14]M. J. Braithwaite, R. W. Joyner, and M. W. Roberts, Discuss. Faraday Soc. 60, 89 (1975).
[15]C. B. Duke, N. O. Lipari, and G. E. Laramore, Nuovo Cimento 23B, 241 (1974); C. B. Duke, private communication.
[16]L. McDonnell, D. P. Woodruff, and K. A. R. Mitchell, Surf. Sci. 45, 1 (1974); D. P. Woodruff, private communication.
[17]The inelastic background at each kinetic energy was assumed to be proportional to the integrated no-loss intensity area at higher energies, as discussed in L. Ley, S. Kowalczyk, R. Pollak, and D. A. Shirley, Phys. Rev. Lett. 29, 1088 (1972); and M. Mehta and C. S. Fadley, *ibid.* 39, 1569 (1977).
[18]P. A. Lee, Phys. Rev. B 13, 5261 (1976).
[19]J. W. Gadzuk, Phys. Rev. B 10, 5030 (1974).
[20]L. McDonnell, D. P. Woodruff, and B. W. Holland, Surf. Sci. 51, 249 (1975).
[21]In treating emission from the substrate core levels $2p_{3/2}$ and $3p$, we make use of the summation over all orbitals in the subshells, which yields a spherically symmetric charge distribution, and further assume that this yields a plane-wave cross section well described by the $\hat{\epsilon}\cdot\hat{k}$ result.
[22]P. A. Lee and J. B. Pendry, Phys. Rev. B 11, 2795 (1975).
[23]See, for example, L. V. Azaroff, *Elements of X-ray Crystallography* (McGraw-Hill, New York, 1968).
[24]C. S. Fadley, Prog. Solid State Chem. 11, 265 (1976).
[25]M. Fink and A. C. Yates, At. Data 1, 385 (1970).
[26]M. Fink and J. Ingram, At. Data 4, 129 (1972).
[27]J. B. Pendry, private communication.
[28]L.-G. Petersson, S. Kono, N. F. T. Hall, C. S. Fadley, and J. B. Pendry, Phys. Rev. Lett. 42, 1545 (1979).
[29]A. Szabo and N. S. Ostlund, J. Chem. Phys. 60, 946 (1974).
[30]L. F. Mattheiss, Phys. Rev. 134, A970 (1964); Phys. Rev. B 10, 995 (1974).
[31]C. J. Powell, Surf. Sci. 44, 29 (1974).
[32]L. F. Wagner, Z. Hussain, C. S. Fadley, and R. J. Baird, Solid State Commun. 21, 453 (1977).
[33]R. J. Reid, Surf. Sci. 29, 623 (1972).
[34]S. Andersson, Solid State Commun. 20, 229 (1976).
[35]D. P. Woodruff, private communication.
[36]S. P. Holland, B. J. Garrison, and N. Winograd, Phys. Rev. Lett. 43, 220 (1979).
[37]P. Hofmann, R. Unwin, W. Wyrobisch, and A. M. Bradshaw, Surf. Sci. 72, 635 (1978), and references therein.
[38]For example, *Crystal Data Determinative Tables*, edited by J. D. H. Donnay and H. M. Ondik, 3rd ed. (U.S. Department of Commerce, MSRDS, National Bureau of Standards and the Joint Committee on Powder Diffraction Standards, Washington, D. C., 1973), Vol. II.
[39]S. Evans, Trans. Faraday Soc. II, Chem. Phys. 71, 1044 (1975).
[40]J. E. Demuth and T. N. Rhodin, Surf. Sci. 45, 249 (1974).
[41]P. M. Marcus, J. E. Demuth and D. W. Jepsen, Surf. Sci. 53, 501 (1975).
[42]B. M. W. Trapnell, Proc. R. Soc. London Ser. A 218, 577 (1953).
[43]A. Ignatjevs, J. B. Pendry, and T. N. Rhodin, Phys. Rev. Lett. 26, 189 (1971).
[44]B. H. Bransden and M. R. C. McDowell, Phys. Rep. 46, 249 (1978).
[45]S. M. Goldberg, S. Kono, N. F. T. Hall, R. J. Baird, and C. S. Fadley, J. Electron Spectrosc. Relat. Phenom. (in press).
[46]A. R. Moon and J. M. Cowley, J. Vac. Sci. Technol. 9, 649 (1972).
[47]R. N. Lindsay, Ph.D. thesis University of Cambridge, 1978 (unpublished) and R. N. Lindsay, C. G. Kinniburgh and J. B. Pendry, J. Electron Spectros. Relat. Phenom. 15, 157 (1979).